Electronic Supplementary Material (ESI) for Nanoscale Advances.

Supporting information for

REGULATING NANOSCALE HEAT TRNSFER WITH JANUS NANOPARTICLES

This PDF file includes:

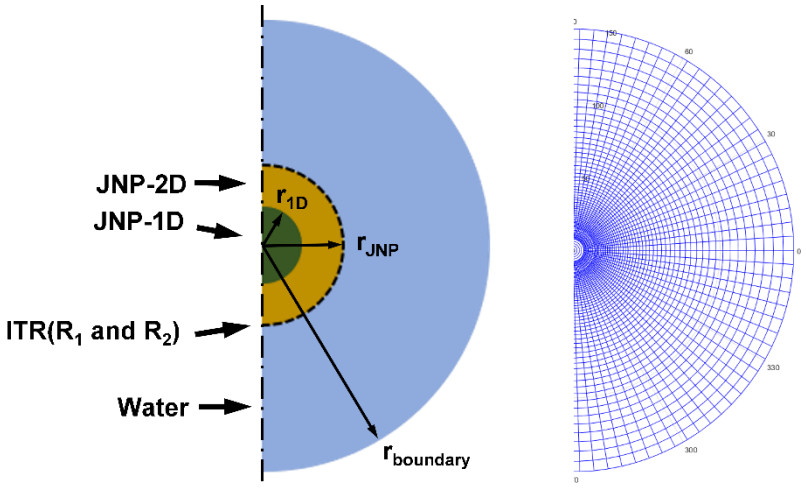

Figure S1. The setup for the FDM model. We expanded the governing equation in spherical coordination and discretized the system with an orthogonal mesh. To separate the singularities in the radius direction and the polar angle direction, we adopt a 1D zone with isothermal in the polar angle direction around the original point. Here we use r_{1D} to denote the size of this 1D zone.

FDM Model validation:

We validated our model by doing a comprehensive mesh dependency analysis. Here, we start with the mesh in the radius and the polar direction for the steady-state model. We assume uniform interfacial thermal resistance (ITR) along the JNP-water interface, thus making a homogenous NP heating where the analytical solution is available. As we have a linear biased mesh grid in the radius direction, we analyzed the truncation error by comparing the FDM results with the analytical solution with different biased mesh factor α ($\Delta r_{i+1} = \alpha \Delta r_i$) and mesh density. The error is calculated by the following equation:

$$error = \frac{abs\left(\Delta T_{analytical} - \Delta T_{FDM}\right)}{\Delta T_{analytical}} \times 100\% \quad \text{(S1)}$$

As shown in Fig. S2A, when α = 1, we have a uniform mesh, and the truncation error drops as we increase the mesh density; when the mesh grid number is 140, the error is around 1%. When α = 1.05, we have a biased mesh, and the error drops much faster as the mesh density increases; when the mesh grid number is 50, the error is around 0.1%. This is because the biased mesh gives a higher mesh density near the JNP where the greatest temperature gradient is observed (Fig. S1), and thus greatly reduces the error and makes the mesh more efficient. As we continuously increase α (α = 1.1), we found that the FDM results become less stable as we increase the mesh density. This might be because the over-biased mesh has coarse mesh grids near the boundary, which can bring extra error. In summary, we validate our model in the radius direction; we found a properly biased mesh factor (α = 1.05) and a mesh density (50, minimum Δr = 0.45 nm); based on this setup, the truncation error is at the order of 0.1%.

Next, we did the mesh independence analysis in the polar angle (θ) direction. Here we introduced a heterogeneous ITR and investigated the temperature contrast ($\frac{\Delta T_1}{\Delta T_2}$) with different mesh densities. Fig. S2B demonstrates that the value of $\frac{\Delta T_1}{\Delta T_2}$ converges as the mesh density increases. Here we assume the results at mesh grid = 275 is the accurate solution, and we calculate the error by comparing the results with this accurate solution (Fig. S2C); we could see the error is at the magnitude of 0.1% for the mesh grid = 100 ($\Delta\theta = \pi/100$).

We chose a truncation error of 0.1% that indicates sufficient accuracy for our mesh set-up; thus, we will keep the set-up (α = 1.05, minimum Δr =0.45 nm, $\Delta\theta = \pi/100$) for the steady-state modeling throughout our paper.

Next, we analyzed the boundary effect. In reality, a free JNP can be treated as a single JNP surrounded by infinite water. In our model, we cannot have an infinite water domain, and the size of the boundary of the water domain can bring error, *i.e.*, boundary effect. Here we calculated the error of boundary effect by comparing the FDM result with a finite boundary radius and the analytical solution with an infinite boundary size. As shown in Fig. S3A, for boundary radius = 3000 nm (200 x r_{JNP}) the error of boundary effect drops to 1%, and we believe this is accurate for our analysis (Fig. S3B). We will keep this set-up throughout our paper.

Finally, we analyzed mesh independence and validated the model in the temporal direction. The spatial mesh set-ups are identical to the steady-state model. Here we plot the FDM results in terms of temporal mesh density (Fig. S4A), we found that the FDM results converge as mesh density increases, and we believe a temporal mesh interval of 0.1 ns can bring sufficiently accurate results. Here we further compared the FDM result with the analytical solution (Fig. S4B),[1] and demonstrated that the FDM results are consistent with the analytical solutions.

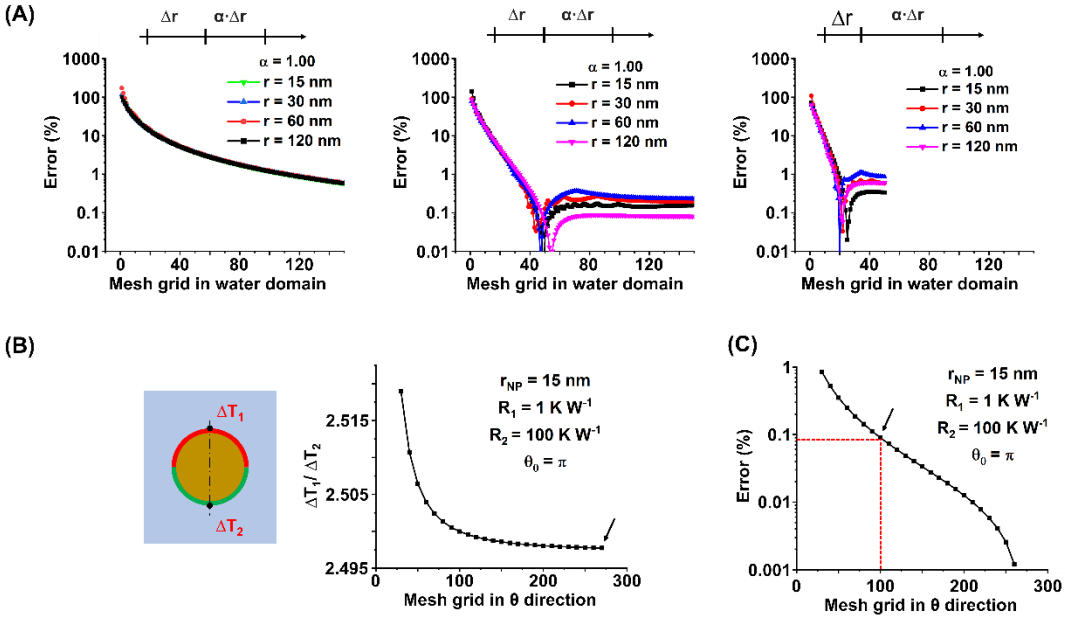

Figure S2. The mesh independence analysis for radius direction. (A) The truncation error in terms of mesh grid number in the radius direction under different biased mesh factor α ($\Delta r_{i+1} = \alpha \Delta r_i$). (B) Temperature contrast in terms of mesh grid number in the polar angle direction. (C) The truncation error in terms of f mesh grid number in the polar angle direction.

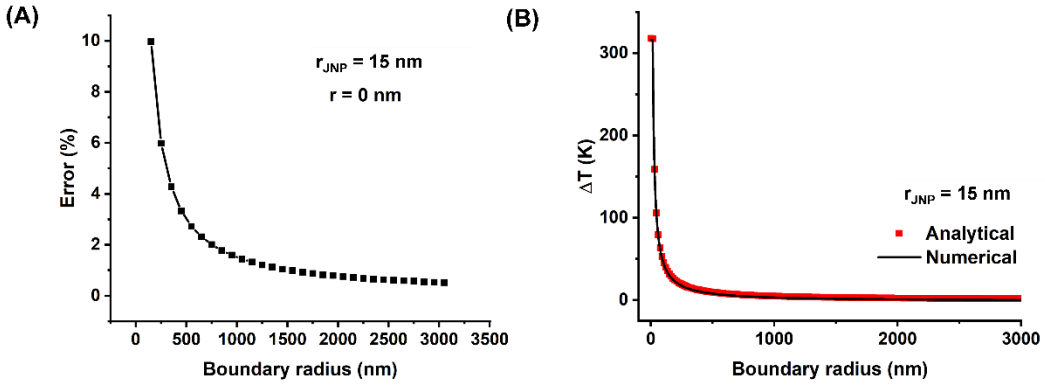

Figure S3. The boundary effect analysis of the FDM model. (A) The error of the temperature rise in JNP by comparing the result with an analytical model that has an infinite boundary size. (B) The temperature profile comparison between the analytical solution with infinite boundary size and FDM result with boundary size = 3000 nm.

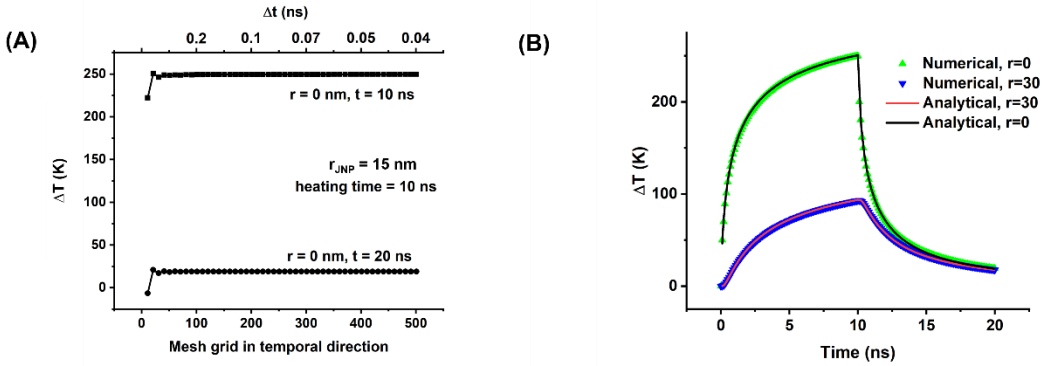

Figure S4. The mesh independence for temporal direction. (A) The mesh independence analysis in the temporal direction. (B) Comparison of FDM results with Δt = 0.1 ns and the analytical solution.

Parallel circuit model

For the parallel circuit model, the thermal transport with JNP can be described with a set of linear equations:

$$\begin{gathered}\left[\frac{1}{R_1}\ -\left(\frac{1}{R_1}+\frac{k_w}{r_{JNP}}\right)\ 0\ \frac{1}{R_1}\ 0\ -\left(\frac{1}{R_2}+\frac{k}{r_{JNP}}\right)\ \left(\frac{A_1}{R_1}+\frac{A_2}{R_2}\right)\ -\frac{A_1}{R_1}\right.\\ \left.-\frac{A_2}{R_2}\right]\left[\Delta T_{JNP}\ \Delta T_1\ \Delta T_2\ \right]=[Q\ 0\ 0\ ] \qquad \text{(S2)}\\ A_1=2\pi {r_{JNP}}^2\left(1-cos(\theta_0)\right)\\ A_2=2\pi {r_{JNP}}^2\left(1+cos(\theta_0)\right)\end{gathered}$$

By solving Equation (S2), we have the temperature rise at the north pole and south pole:

$$\begin{gathered}\left[\Delta T_{JNP}\ \Delta T_1\ \Delta T_2\ \right]\\ =\left[\frac{Q\left(r_{JNP}+R_1k\right)\left(r_{JNP}+R_2k\right)}{A_1kr_{JNP}+A_2kr_{JNP}+A_1k^2r_{JNP}+A_2k^2r_{JNP}}\ \frac{Qr_{JNP}\left(r_{JNP}+R_2k\right)}{A_1kr_{JNP}+A_2kr_{JNP}+A_1k^2r_{JNP}+A_2}\right. \qquad \text{(S3)}\end{gathered}$$

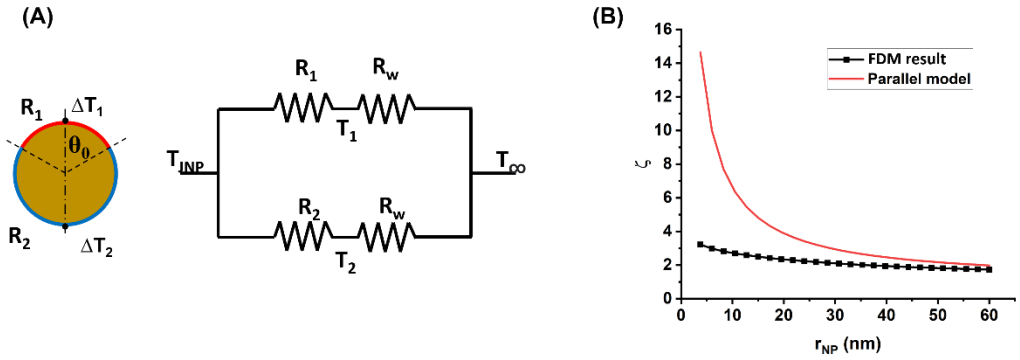

Figure S5. The parallel circuit model for the JNP heating under steady state.

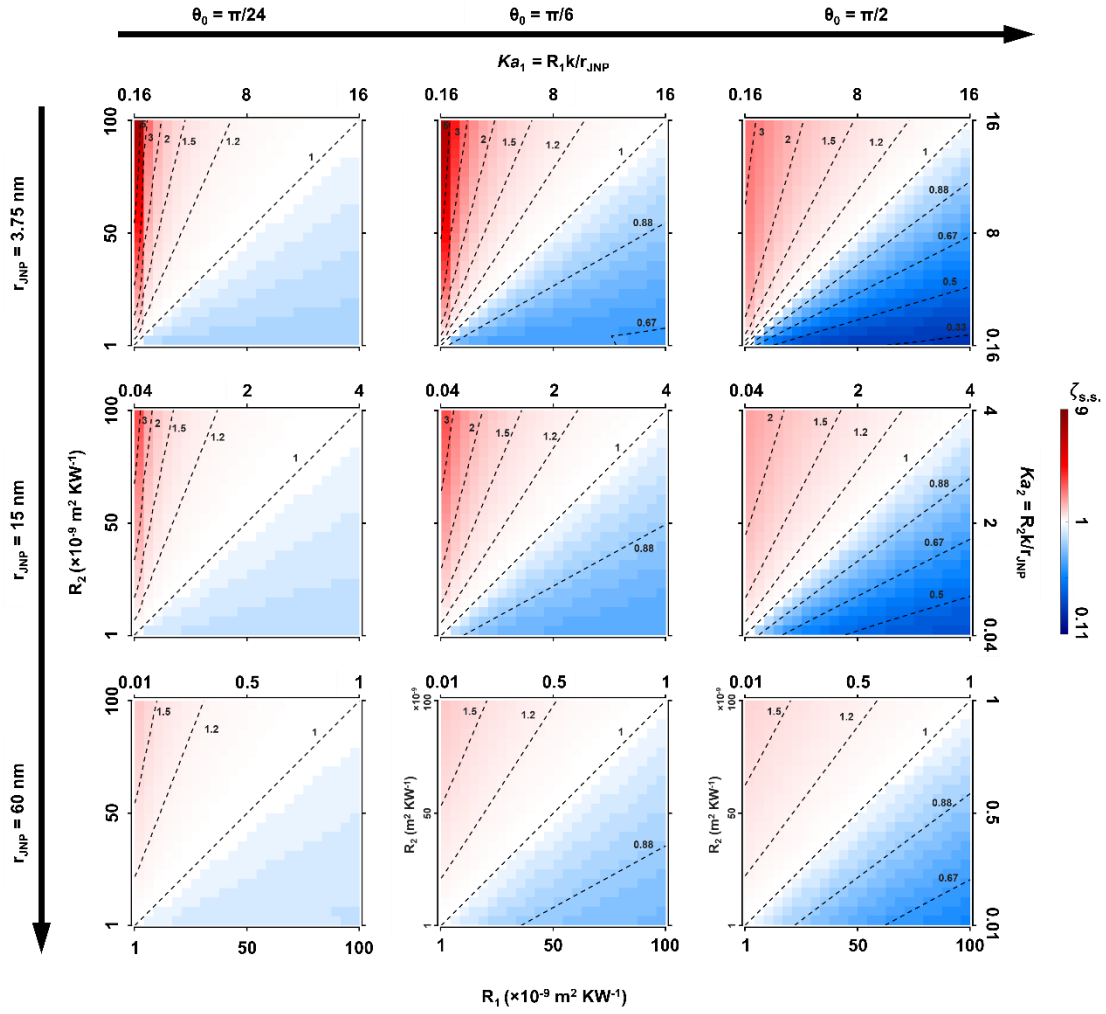

Figure S6. $\zeta_{s.s.}$ map in terms of R_1 and R_2 with different r_{JNP} and θ_0.

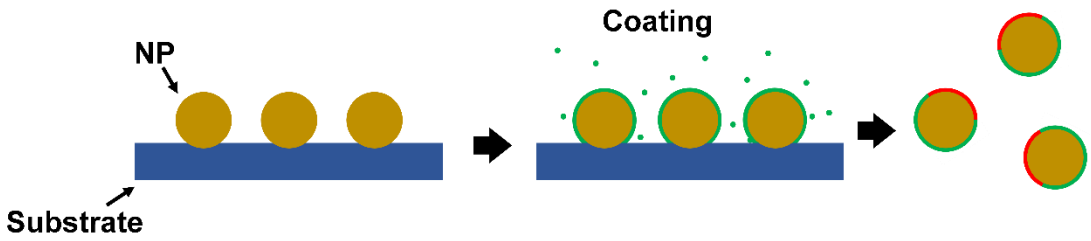

Figure S7. Schematic illustration of the synthesize protocol for JNP.

Table S1. Interfacial thermal resistance (ITR) from previous reports.

Nano structure	material	solvent	Interfacial ligand	ITR $\times 10^9$ m^2KW^{-1}	Reference
NP	Pt	Water	No	16.1	[2]
NP	AuPt	Water/alcohol	Tiopronin	5-11.1	[3]
			Thioalkylated	2.9-6.3	
NP	Au	Water	Citrate	8.3-11.1	[4]
Flat surface	Au	water	C18	18.2-22.2	[5]
NR	Au	water	CTAB	2.2-7.7	[6]
NP	Au	water	No	5.9-6.7	[7]
Flat surface	Au	Water	n-undecanethiol (n ¼ 11–18)	14.3-16.7	[8]
			Methyl 3-mercaptopropionate	6.5-8.0	
			11-Mercapto-1-undecanol	4.5-6.3	
NR	Au	Water	CTAB	12	[9]
			PEG	4.4	
Nanotube	Carbon	D_2O	Polystyrene sulfonate surfactant	83.3	[10]

Reference:

1. Goldenberg H, Tranter CJ. Heat flow in an infinite medium heated by a sphere. Br J Appl Phys. 1952;3: 296.

2. Wilson OM, Hu X, Cahill DG, Braun PV. Colloidal metal particles as probes of nanoscale thermal transport in fluids. Phys Rev B Condens Matter. 2002;66: 224301.

3. Ge Z, Cahill DG, Braun PV. AuPd Metal Nanoparticles as Probes of Nanoscale Thermal Transport in Aqueous Solution. J Phys Chem B. 2004;108: 18870–18875.

4. Plech A, Kotaidis V, Grésillon S, Dahmen C, von Plessen G. Laser-induced heating and melting of gold nanoparticles studied by time-resolved x-ray scattering. Phys Rev B Condens Matter. 2004;70: 195423.

5. Ge Z, Cahill DG, Braun PV. Thermal conductance of hydrophilic and hydrophobic interfaces. Phys Rev Lett. 2006;96: 186101.

6. Schmidt AJ, Alper JD, Chiesa M, Chen G, Das SK, Hamad-Schifferli K. Probing the Gold Nanorod−Ligand−Solvent Interface by Plasmonic Absorption and Thermal Decay. J Phys Chem C. 2008;112: 13320–13323.

7. Merabia S, Shenogin S, Joly L, Keblinski P, Barrat J-L. Heat transfer from nanoparticles: a corresponding state analysis. Proc Natl Acad Sci U S A. 2009;106: 15113–15118.

8. Harikrishna H, Ducker W, Huxtable S. The influence of interface bonding on thermal transport through solid–liquid interfaces. Appl Phys Lett. 2013;102: 251606.

9. Wu X, Ni Y, Zhu J, Burrows ND, Murphy CJ, Dumitrica T, et al. Thermal Transport across Surfactant Layers on Gold Nanorods in Aqueous Solution. ACS Appl Mater Interfaces. 2016;8: 10581–10589.

10. Huxtable ST, Cahill DG, Shenogin S, Xue L, Ozisik R, Barone P, et al. Interfacial heat flow in carbon nanotube suspensions. Nat Mater. 2003;2: 731–734.